analytical chemistry

pubs.acs.org/ac Article

Novel Isotope-Coded Photochemical Derivatization Coupled with LC-MS and MS Imaging Platform Enables Sensitive Quantification and Accurate Localization of Amine Submetabolome in Pancreatic Disease

Yaling Wu,[¶] Manjiangcuo Wang,[¶] Rui Wang, Shan Yang, Wanmeng Li, Siwei Bi, Xia Li, Yangjuan Bai, Qing Xia, Huimin Lu,* Chenggong Hu,* and Dan Du*

Cite This: *Anal. Chem.* 2025, 97, 6611−6619 Read Online

ACCESS | Metrics & More | Article Recommendations | Supporting Information

ABSTRACT: Alterations in amine metabolite levels are closely associated with the poor progression of pancreatic disease, including acute pancreatitis (AP) and pancreatic cancer (PC). However, effectively quantifying and visualizing these metabolites through mass spectrometry (MS) has proven to be challenging. Here, we have designed a novel and rapid strategy for analyzing the amine submetabolome within liquid chromatography−mass spectrometry (LC-MS) and air-flow-assisted desorption electrospray ionization mass spectrometry imaging (AFADESI-MSI) platforms by inducing a pair of isotope-labeling-based photochemical derivatization reagents. The simultaneous introduction of a 4-amino-1-methylpyridinium moiety renders a 160- to 1037-fold higher response in MS. Coupled with full MS-ddMS^2 and precursor ion scan modes, this labeling strategy allows for straightforward detection of 423 peaks for indazolone derivatives and identification of 82 amine metabolites in biological samples. The semiquantitation of the 82 amines in plasma from AP patients and healthy controls resulted in the discovery of unreported aromatic amines and aminoaldehydes with significant changes in AP and employing ethanolamine for distinguishing the severities of AP in the early stage. In the MSI platform, the photochemical reagent can efficiently derivatize primary amine metabolites avoiding spatial deviation and significantly enhancing imaging sensitivity in rat brain and kidney. Further joint analysis of amine submetabolome in plasma and pancreas from PC patients by use of these two platforms allowed for identifying the significant metabolite, methylamine. These results together enhance the role of amine-driven biomarker discovery in the diagnosis of pancreatic disease and accelerate the application of on-tissue photochemical derivation in MSI.

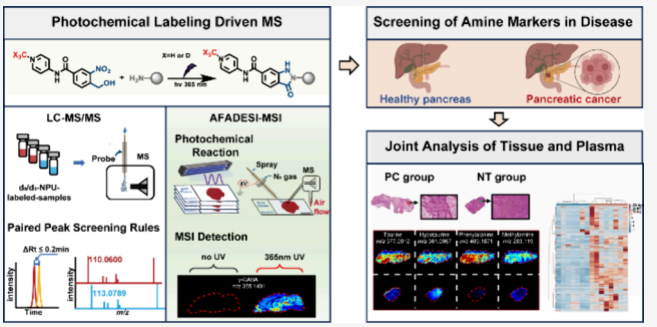

INTRODUCTION

The amine submetabolome, including amino acids, aliphatic amines, small peptides, neurotransmitters, and a series of amine metabolites, regulates important biological functions in organisms.[1] A panel of amine metabolites is promising for the early diagnosis of pancreatic disease. Severe acute pancreatitis (SAP), accounting for one-fifth of total AP patients, is often characterized by pancreatic necrosis, systemic complications, and multiorgan failure, resulting in a high mortality rate of 20−40%, without effective predictors.[2] The level of blood urea nitrogen or basic amino acids, which are reflective of nitrogen metabolic disarray in the pancreas is essential for diagnosing SAP at an early stage.[3] Pancreatic cancer (PC), a leading cause of cancer-related deaths worldwide, is mostly diagnosed at a late stage, resulting in the lowest 5-year survival rate (13%) among all cancers.[4,5] Its common biomarker carbohydrate antigen 19-9 lacks specificity.[6] It is necessary to look for biomarkers sharing changes in both *in situ* and peripheral circulation. The amino acids,[7] polyamines,[8] and carnitines[9] are all involved in the pathogenesis and progression of this disease. Hence, rapid, broad, and sensitive detection of the amine submetabolome in biofluids and visualization of spatial distributions of these metabolites in tissues will be crucial in developing new diagnostic strategies for pancreatic disease.

Liquid chromatography−mass spectrometry (LC-MS) is considered a suitable technology for profiling amines in complex matrices. The detection of amine metabolites is typically performed in positive mode analysis,[10] whose sensitivity and accuracy are always impacted by peak shape

Received: November 26, 2024
Revised: March 4, 2025
Accepted: March 7, 2025
Published: March 18, 2025

https://doi.org/10.1021/acs.analchem.4c06388
Anal. Chem. 2025, 97, 6611−6619

and instability.[11] In addition, the amino acids, aliphatic amines, aromatic amines, small peptide, catecholamines, and lysophosphatidylethanolamine (LPE) exhibit varying polarities, which makes it challenging to detect and quantify them simultaneously. In-solution chemical derivatization (ISCD) offers an opportunity to improve the overall analytical performance in LC-MS. One common strategy to improve the coverage and sensitivity of amine metabolites is to react with positively charged and hydrophobic groups. Derivatization reagents like benzoyl chloride, dansyl chloride, 3,5-bis(trifluoromethyl) phenyl isothiocyanate, and 6-aminoquinolyl-*N*-hydroxysuccinimidyl carbamate have demonstrated their effectiveness in detecting amine metabolites.[12] Moreover, the stable isotope-labeled (SIL) approach, which employs an isotope tag parallel with the chemical derivatization, greatly improves coverage and quantitative accuracy of analytes. For example, ^{12}C-/^{13}C-isotope dansylation labeling of metabolites has been applied to quantification of amino acids.[13] A pair of 6,7-dimethoxy-3-methyl isochromenylium tetrafluoroborate ([d_0/d_6]-DMMIC) was used for analysis of differential amine submetabolomes between the carcinoma and paracarcinoma tissues of esophageal squamous cell carcinoma.[14] As a limitation, these derivatizing reagents often require the use of organic or inorganic bases, leading to potential quenching and contamination issues. Recent advancements in photochemical derivatization methods, characterized by their catalyst-free, environmentally friendly, and high efficiency, have garnered increasing attention.[15] However, there are limited reports on photosensitive probes designed for the amine submetabolome.

Mass spectrometry imaging (MSI) can identify, localize, and relatively quantify compounds by directly scanning the sample surface.[16] It can also be combined with on-tissue chemical derivatization (OTCD) to achieve a rapid and highly sensitive visualization for target compounds.[17] A variety of sampling ionization methods have been employed for MSI, such as secondary ion mass spectrometry (SIMS), matrix-assisted laser desorption/ionization (MALDI), and desorption electrospray ionization (DESI).[18] The OTCD-MALDI-MSI analysis method with relatively high spatial resolution achieves *in situ* sensitization and analysis of amine metabolites by designing reactive matrix or precoating derivatization reagents, but the complex synthesis route of reactive matrix or potential matrix-reagent reaction interference remains the main factor limiting the development of analytical methods. DESI-MSI does not require the matrix to participate in the ionization, and the solvent environment provided during desorption can further improve the chemical reaction efficiency and is more suitable for the development of OTCD methods.[19] The introduction of photochemical reaction not only reduces the number of times the reagent is coated but also further simplifies other *in situ* labeling processes, avoiding the spatial displacement of metabolites. The OTCD-MSI research driven by photochemical reactions may be a new approach for rapid detection and sensitive analysis of metabolites in complex diseases.

Herein, we report the design and synthesis of a new type of photochemical probe used for ISCD and OTCD of amine metabolites in plasma and frozen tissue sections, respectively. The simultaneous introduction of a 4-amino-1-methylpyridinium moiety in a photochemical probe renders a 160- to 1037-fold higher response in LC-MS, and the SIL approach coupled with two distinctive MS scanning modes enlarges the scope of primary amine submetabolome, allowing for quantitation of 82 amine metabolites in biological samples. Furthermore, this light-activated probe design permits mapping amine metabolites in complex biological tissues by air-flow-assisted desorption electrospray ionization mass spectrometry imaging (AFADESI-MSI), without heating, analyte dislocation, and degradation. The optimized OTCD approach allowed us to derivatize 43 metabolites from brain tissue and 45 metabolites from kidney tissue. Importantly, we applied the two methods to reveal the differential metabolites in plasma and tissue for SAP and PC early diagnosis. This strategy significantly broadens the scope and depth of amine metabolite analysis, especially overcoming the limitations encountered by previous strategies in OTCD-DESI-MSI.

EXPERIMENTAL SECTION

Chemicals and Reagents. LC/MS-grade methanol (MeOH), acetonitrile (ACN), formic acid, and HPLC-grade dichloromethane were purchased from Fisher Scientific (Pittsburgh, PA, USA). *N*,*N*-Diisopropylethylamine (DIPEA), 4-bromomethyl-3-nitrobenzoic acid, o-(7-azabenzotriazol-1-yl)-*N*,*N*,*N*′,*N*′-tetramethyluronium hexafluorophosphate (HATU), 4-aminopyridine, iodomethane (CH_3I), and iodomethane-d_3 (CD_3I) were purchased from Innochem (Beijing, China). All standards were purchased from Sigma-Aldrich (St. Louis, MO, USA), Alfa Aesar (Pittsburgh, PA, USA), Innochem (Beijing, China), Apinno (Beijing, China), and Targetmol (Beijing, China). Ultrapure water was obtained from Milli-Q (Merck Millipore, Darmstadt, Germany).

Synthesis of 4-(4-(Hydroxymethyl)-3-nitrobenzamido)-1-methylpyridinium iodide (d_0-NPU) and 4-(4-(Hydroxymethyl)-3-nitrobenzamido)-1-(methyl-d_3) pyridinium iodide (d_3-NPU). The detailed information is available in the Supporting Information.

Sample Preparation. Sample preparation for LC-MS analysis: tissue samples were prepared according to the guidelines described before. Frozen tissue was weighed (~50 mg) and homogenized in a 1.5 mL precooled mixture of MeOH/H_2O (1:1) within a 2 mL Eppendorf tube. Centrifuged at 13,000 rpm for 10 min at 4 °C. The supernatant was collected and transferred to a new 5 mL Eppendorf tube. The pellet was retained in the tube on ice for organic solvent extraction. The homogenization extraction step was repeated using a precooled mixture of dichloromethane/MeOH (3:1) in a 1.5 mL volume. The centrifugation step was repeated once. Finally, the supernatants from both extractions were combined and dried in a vacuum concentrator (Christ, Germany). A total of 50 μL of cerebrospinal fluid (CSF), urine, or plasma was separately added to 200 μL of cold MeOH, vortexed for 30 s, and then placed at −20 °C for 1 h. Subsequently, the samples were centrifuged at 1000 g for 10 min at 4 °C to precipitate proteins and dried in a vacuum concentrator.

Sample preparation for MSI analysis: All the frozen tissues were cut into 10 μm-thick sections using a cryostat microtome (CM 1950, Leica Microsystems, Wetzlar, Germany) at a chamber temperature of −20 °C. Two consecutive sections were adjacently thaw-mounted on the same Superfrost Plus microscope slide (Thermo Fisher Scientific, San Jose, CA, USA). Neighboring sections were acquired for hematoxylin-eosin (H&E) staining and stored at −80 °C. Tissue sections were desiccated at room temperature for 20 min before derivatization.

In-Solution and On-Tissue Derivatization. For in-solution derivatization, a solution of d_0-NPU or d_3-NPU (1 mM) was prepared with PBS/MeOH (1:1, pH = 10).

https://doi.org/10.1021/acs.analchem.4c06388
Anal. Chem. 2025, 97, 6611−6619

Subsequently, standards, tissue extract, or biofluid extract were separately added to the d_0-NPU or d_3-NPU solution and exposed to 365 nm UV light for 30 min. The samples were collected, diluted with MeOH/H_2O (1:1), and centrifuged at 13,000 rpm for 10 min. The supernatant was then collected for LC-MS/MS analysis.

For on-tissue derivatization, d_0-NPU or d_3-NPU (5 mg, 0.017 mmol) was dissolved in PBS/MeOH (1:1, pH = 10). The reagent was sprayed onto the surface of dried tissue sections using a TM-Sprayer (HTX Technologies, Carrboro, NC, USA). The spraying conditions were set as follows: a spraying temperature of 70 °C, flow rate of 30 μL/min, nozzle height of 40 mm, nitrogen pressure of 10 psi, and gas pressure rate of 10 psi for 6 cycles, drying time of 8 s, track speed of 800 mm/min, and track spacing of 3 mm. After spraying, the sections were exposed to 365 nm UV light for 30 min.

LC-MS Analysis and AFADESI-MSI Analysis. High resolution mass spectrometry (HRMS) experiments were performed on a Vanquish Flex system (Thermo Fisher Scientific, San Jose, CA, USA) connected to a Q-Exactive Plus Orbitrap mass spectrometer (Thermo Fisher Scientific, Waltham, MA, USA). The separation was performed on a Waters ACQUITY UPLC HSS T3 column (100 × 2.1 mm, 1.8 μm particle size) from Waters Corporation. The column temperature was kept at 45 °C. Ultrapure water containing 0.1% formic acid and acetonitrile was used as mobile phases A and B, respectively, with a flow rate of 0.15 mL/min. The autosampler was operated at 7 °C with an injection volume of 2 μL. The gradient elution program was set as follows: 0−20 min, 2−100% B; 20−25 min, 100% B; 25−25.1 min, 2% B; and 25.1−30 min, 2% B.

The MSI experiments were performed using an AFADESI-MSI platform coupled with a Q-Exactive Plus Orbitrap mass spectrometer. The AFADESI-MSI platform included a sprayer, syringe pump, stainless-steel transport tube, vacuum pump (MZ2C NT, Vacuubrand, Wertheim, Germany), and SC100 series stepper motor (Beijing Optical Century Instrument Factory, Beijing, China). The AFADESI-MSI platform parameters were set as follows: tube extracting gas flow, 45 L/min; spraying solvent, ACN/H_2O (8:2, v/v); flow rate, 5 μL/min; spraying gas, 0.7 MPa nitrogen; and spray voltage, 7.0 kV. The scan speed on the *X*-axis of the 3D electrical moving stage was 0.2 mm/s, and the vertical step on the *Y*-axis was 0.2 mm. HRMS data were acquired in positive mode. The MS parameters were set as follows: the capillary temperature was set to 350 °C; sheath gas, 40 arb; aux gas, 5 arb; auxiliary gas heater temperature was maintained at 220 °C; and spray voltage, 3.5 kV. Data-dependent MS^2 assays comprised a full scan (m/z 200−800; resolution, 70,000; AGC target, 3e6; maximum IT, 100 ms) and an MS/MS scan (resolution, 17,500; AGC target, $1e^5$; maximum IT, 50 ms; loop count, 15; NCE, 20, 40, and 60).

The precursor ion scan (PIS) method and quantification experiment were performed on a SCIEX Exion LC UHPLC system connected to a triple quadrupole (QqQ) 5500 (QTRAP 5500) mass spectrometer (AB SCIEX, Foster City, CA, USA). For the PIS method, the HPLC separation column and mobile phase gradient were the same as those of the full scan method by HRMS. The PIS method consists of two precursor ions (m/z 110.1 and 113.1) in the mass range of m/z 200−800 and a scan rate of 200 Da/s. The optimized MS parameters were set as follows: ion spray voltage, 4.0 kV; source temperature, 650 °C; curtain gas, 35; CAD gas, 8; ion source gas 1, 50; ion source gas 2, 40. The quantification was carried out by multiple reaction monitoring (MRM) mode. Waters ACQUITY UPLC HSS T3 column (100 mm × 2.1 mm, 1.8 μm particle size) was used for LC-MS/MS analysis. The column temperature was kept at 45 °C. Ultrapure water and 0.1% formic acid in MeOH were used as mobile phases A and B, respectively, with a flow rate of 0.15 mL/min. The autosampler operated at 7 °C with an injection volume of 2 μL. The gradient elution program was set as follows: 0−20 min, 10−100% B; 20−25 min, 100% B; 25−25.1 min, 10% B; 25.1−30 min, 10% B. The MS parameters were the same as those for the LC-PIS-MS method. The dwell time was set at 4 ms for each ion transition, and Table S1 summarizes the MRM conditions for each compound. Data acquisition was performed in positive ion mode.

Additional information regarding materials and methods for method optimization, method validation, homogenate strip preparation, data analysis, and ethics can be found in the Supporting Information.

RESULTS AND DISCUSSION

Design and Synthesis of the Derivatization Reagent NPU. To develop this photochemical derivatization strategy in LC-MS (Figure 1A and B), we first synthesized 4-(hydroxymethyl)-3-nitrobenzoic acid (**2**)[20] through alkaline hydrolysis of 4-(bromomethyl)-3-nitrobenzoic acid (**1**). Then, we incubated 4-aminopyridine with **2** to produce 4-(hydroxymethyl)-3-nitro-N-(pyridine-4-yl) benzamide (**3**) to increase MS ionization efficiency. Lastly, we incorporated CH_3I and CD_3I to perform methylation at the *N*1 position of pyridine to further improve positive charge and obtained 4-(4-(hydroxymethyl)-3-nitrobenzamido)-1- methylpyridinium iodide (d_0-**NPU**) and 4-(4-(hydroxymethyl)-3-nitrobenzamido)-1-(methyl-d3) pyridinium iodide (d_3-**NPU**), respectively (Figure 1C). Both d_0-NPU and d_3-NPU could be characterized by chemical shift and integration of hydrogen on the *N*-substituted methyl group in the ^{1}H NMR spectrum (Figure 1D). Furthermore, d_0/d_3-NPU exhibits stable and high-abundance product ion at m/z 110.0600 and 113.0789, respectively, which was possibly assigned to intramolecular 1,3-OH- shift in 4-formamido-1-methylpyridinium iodide, ultimately resulting in the cleavage of d_0/d_3-NPU to form 4-hydroxy-1-methylpyridinium iodide ($C_6H_8NO^+$) (Figure 1E and Figure S1). Thus, the ion pair 110.0600/113.0789 can be used in the qualitative and quantitative profiling of amines in d_0/d_3-NPU-derivatized samples. It should be mentioned that the pair of isotope-coded photochemical reagents d_0/d_3-NPU is unique for the identification of the amine submetabolome, since stable fragment ions are not always present in other derivative photochemical reagents. For example, we previously synthesized 4-(hydroxymethyl)-3-nitro-N-(pyridin-4-ylmethyl) benzamide (**NMP**) for the derivatization of amine metabolites (Scheme S1), but the MS/MS spectra of the derivatized amines did not yield stable reporter ions.

Investigation and Optimization of NPU Derivatization for LC−MS Analysis. To optimize the reaction efficiency with amines, we treated d_0-NPU with 12 different standards at various pH, irradiation time, incubation time, temperatures, concentrations, and wavelengths (Figure S2 and S3). As a result, the pH value of the reaction system plays an important role in influencing the derivatization efficiency in comparison to other reaction conditions, such as temperature and incubation time. The concentration of the photochemical

https://doi.org/10.1021/acs.analchem.4c06388
Anal. Chem. 2025, 97, 6611−6619

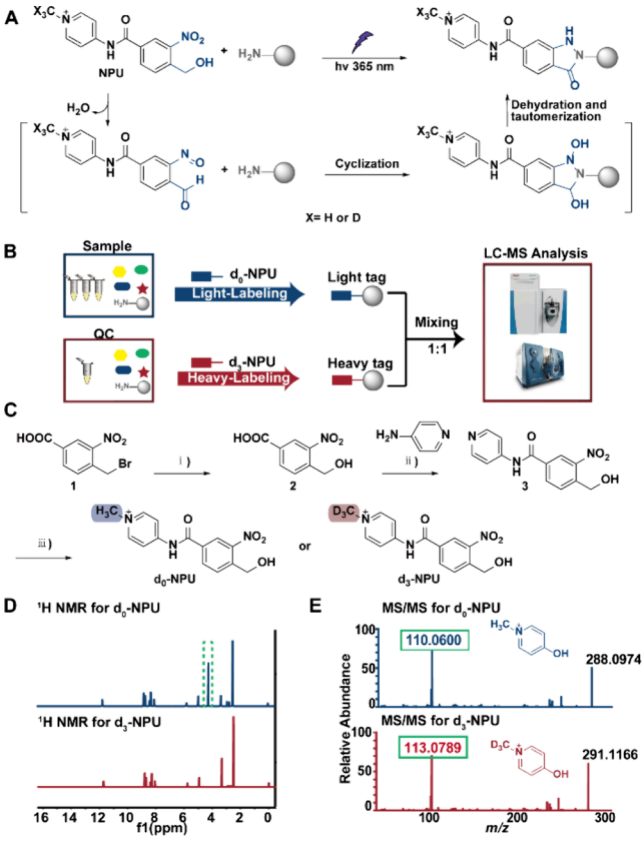

Figure 1. A) General scheme for light-induced indazolone formation. B) Workflow of the isotope-coded photochemical derivatization LC-MS technique for in-depth quantification of the amine submetabolome in metabolomics. C) The synthesis of d_0-NPU and d_3-NPU. Reagents and conditions: (i) Na_2CO_3 1.2 equiv, acetone/H_2O (1:1), 75 °C, 5 h. (ii) 2, 4-Aminopyridine 3 equiv, HATU 1.2 equiv, DIPEA 3 equiv, DMF, room temperature (r.t.), overnight. (iii) CH_3I/CD_3I 3 equiv, DMF, r.t, overnight. D) The ^{1}H NMR (DMSO-d_6, 400 MHz) spectrum of d_0-NPU and d_3-NPU. E) The LC-HRMS/MS spectra of the d_0-NPU and d_3-NPU.

reagent was optimized at 1 mM for most of the standards. Thus, the derivatizing method was optimized as follows: 1 mM of d_0-NPU was added to amine metabolites in PBS (pH = 10) buffer and irradiated for 30 min using a light wavelength of 365 nm, at room temperature (25 °C). Moreover, the MS intensities of eight representative amines including glycine (Gly), alanine, taurine, spermine, ethylamine, ethanolamine (ETA), *o*-phosphocolamine and LPE (18:1) were compared between the derivatization and common measurement. The results revealed a significant increase in MS intensities by 160−1037 times when compared to common measurement techniques (Figure S4). Especially, ethylamine, ETA, *o*-phosphocolamine, and LPE (18:1) were detected only in LC-MS by derivatization (Table S2). At the same time, we further evaluated the conversion rate of the reaction by derivatization of ETA and Gly, and found that the reaction conversion rates were 99.4% and 99.6%, respectively, and no additional side reactions were observed in MS, further illustrating the excellent performance of the photochemical reaction (Figure S5). All d_0-/d_3-labeled amines displayed product ions at m/z 110.0600 and 113.0789 (Figure S6), which serve as characteristic product ions for the detection of all amine metabolites. Further method validation results indicated the LOD is between 0.03 to 5.0 nM, and the presence of a good linearity (R^2 between 0.9977 and 0.9999), precision (interday: 4.44−13.1%; intraday: 1.75−9.29%), accuracy (recovery: 82.6−108.9%) and stability (1.77−14.2%) (Figure S7, Tables S3 and S4), making them ideal for continuous analysis of large-scale samples.

Workflow of Isotope-Coded Photochemical Derivatization in LC-MS. Next, we utilized two distinctive MS scan modes to identify more amine metabolites with characteristic pair ions (Figure S8). The d_0-NPU and d_3-NPU were respectively added to half of pancreatic samples and subsequently mixed in a 1:1 ratio for LC-HRMS/MS analysis. One total ion chromatogram (TIC) was obtained under the full MS-ddMS^2 mode in Q-Orbitrap, which indicated many peak pairs with a mass difference of 3.0178 Da assigned to various NPU-labeled amine metabolites (Figure 2A). These

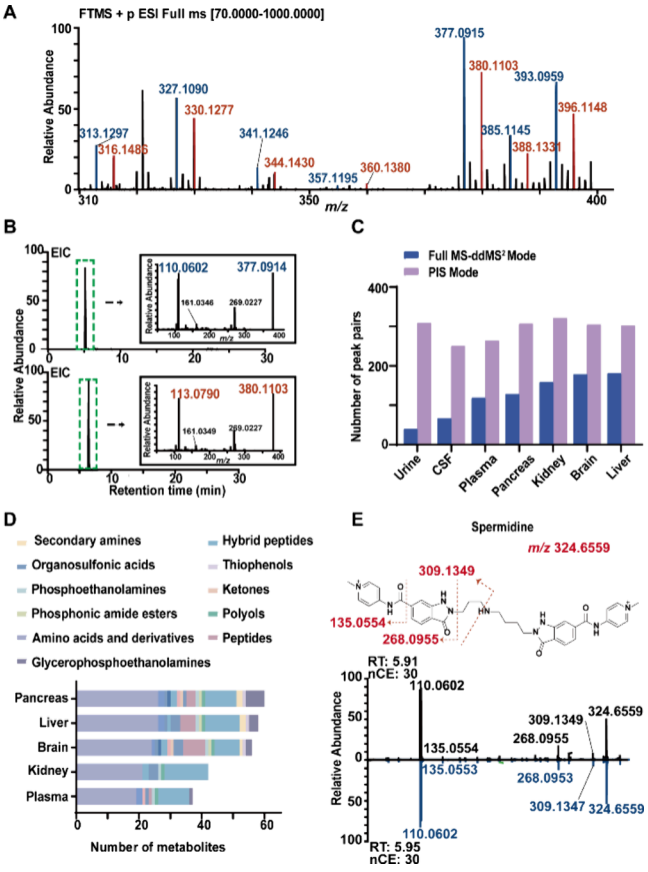

Figure 2. A) The LC-HRMS spectrum for d_0/d_3-NPU labeled mouse pancreatic tissue (2-fold magnification at m/z 300−400). B) The extracted ion chromatogram (EIC) and LC-HRMS/MS spectra for m/z 377.0914 (t_R = 6.03) and m/z 380.1104 (t_R = 6.03). C) Peak pairs from d_0/d_3-NPU labeled multiple tissue and biofluid samples under full MS-ddMS^2 scan in Q-Orbitrap and PIS mode in QqQ, respectively. D) Overview of the classes of amine metabolites covered by the isotope-coded photochemical derivatization strategy in various biological tissues. E) The LC-HRMS/MS spectra illustration of d_0-NPU labeled sample (upper) and standard (below) for spermidine.

NPU-labeled metabolites have both product ions m/z 110.0600 and 113.0789 at the same retention time, such as the metabolite at t_R = 6.03 min (Figure 2B). The NPU labeled pancreatic samples (1/1, v/v) were further analyzed by LC-QqQ/MS with the PIS mode under the same chromatography conditions. Two individual TICs were acquired by monitoring

https://doi.org/10.1021/acs.analchem.4c06388
Anal. Chem. 2025, 97, 6611−6619

the product ions m/z 110.1 and 113.1. Compared to the single MS under the full MS-ddMS^2 mode in Q-Orbitrap, the light-labeled and heavy-labeled samples can be clearly distinguished in two separate TICs under the PIS mode in the QqQ. The selectivity and sensitivity are greatly improved due to the elimination of interference from the other unlabeled compounds in PIS (Figure S9). Moreover, several labeled metabolites could be detected only in PIS mode, such as m/z 324.65 (Figure S9). Taken together, the combination of two scan methods can significantly improve the identification of quasi-molecular ions of the amine metabolites, benefiting the further elucidation of their structures.

Determination of Metabolites in Various Biological Tissues by LC-MS. To obtain more peak pairs in full MS-ddMS^2 mode with the given retention time as in the PIS mode used for compound identification in database, various samples including the liver, brain, kidney and pancreas of mice as well as the plasma, urine and CSF of human were used for labeling and analysis by LC-MS/MS (Figure 2C). Subsequently, a total of 423 peak pairs with product ion m/z 110.0600/113.0789 were detected from all the d_0/d_3-NPU labeled biological samples under full MS-ddMS^2 mode in Q-Orbitrap. We calculated the accurate mass of metabolites by subtracting the mass of NPU and determined 82 of them using Human Metabolome Database (HMDB) with a mass accuracy tolerance of 5 ppm based on an in-house Python-based code.[21] We also note that all of these matched and identified metabolites are attributed to primary amine metabolites, and no secondary amine metabolites, thiol, or hydroxyl metabolites have been identified. This observation is consistent with the proposed reaction mechanism (Figure 1A), which involves the formation of key intermediates under light activation, subsequently reacting with primary amines through cyclization, dehydration, and isomerization to form indazolone derivatives. Compared to primary amines, thiols and hydroxyl groups, due to their lower nucleophilicity or difficulty in forming stable cyclic intermediates, hinder the reaction progress. Additionally, aromatic amines, due to the presence of the aromatic ring, exhibit lower nucleophilicity and suffer from steric hindrance, resulting in an extremely low reaction efficiency. Therefore, this reaction is particularly selective for primary amines. Further, these amine metabolites with different polarities were categorized using ClassyFire (Figure S10), such as amino acids, peptides, polyamines, aromatic amines, and glycerophosphoethanolamines, exhibited different types and abundances across each biological sample (Figure S11).

Among them, the class of amine metabolites is the most abundant in the pancreas (Figure 2D). The structures of the metabolites were further identified by comparing the retention time and mass spectrum of 24 standards in the LC-MS/MS analysis (Figure 2E and Figure S12). The ion source parameters for QqQ/MS and the extraction method were optimized based on peak areas of 82 metabolites (Figure S13). Lastly, we established an LC-QqQ/MS method consisting of 82 precursor ions and 164 product ions (Table S1).

Amine Submetabolome Profiling in the Plasma of AP Patients and Healthy Controls. The proposed method was further applied for the determination of the amine submetabolome in the plasma of AP patients and healthy controls (HCs), with demographic characteristics outlined in Table S5. The human samples were labeled with d_0-NPU, and the pooled plasma was regarded as QC samples were heavy labeled with d_3-NPU. Then the light and heavy labeled samples with the same volume were mixed, followed by LC-QqQ/MS analysis. The relative quantitation was calculated based on the peak area ratio of d_0-NPU derivatized amine metabolites and their corresponding d_3-NPU derivatized amine metabolites. Principal component analysis (PCA) showed HCs clustered apart from AP patients (Figure 3A), and more than half of

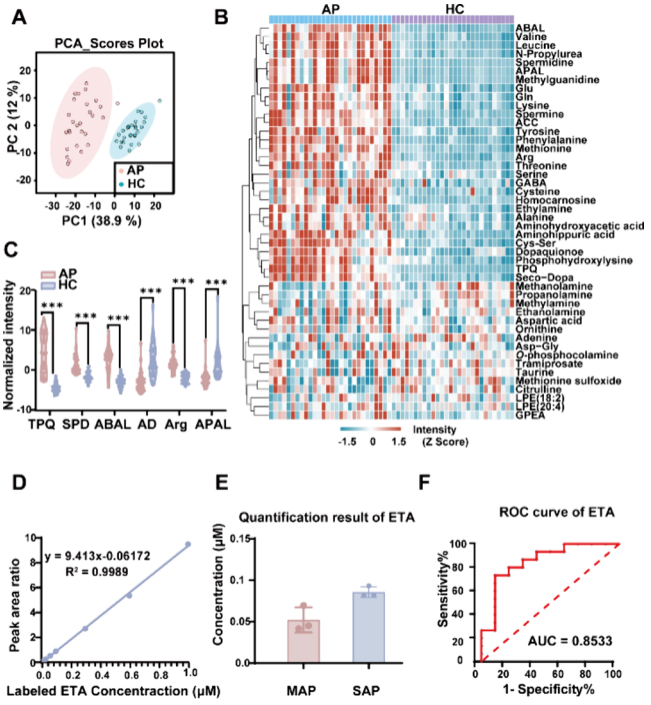

Figure 3. A) 2D score plot for AP and HC groups by principal component analysis (PCA). B) Heatmap of amine metabolites in acute pancreatitis (AP, n = 28) and healthy control (HC, n = 28) plasma. Metabolite intensities are Z-score normalized. C) Violin plots of six significantly dysregulated metabolites (t-test, FDR-adjusted p < 0.05): topaquinone (TPQ), spermidine (SPD), aminobutyraldehyde (ABAL), adenine (AD), aminopropionaldehyde (APAL), and arginine (Arg). D) Calibration curve of the d_0/d_3-NPU-derivatized ETA. E) Quantification results of ETA in plasma samples from mild acute pancreatitis (MAP) and severe acute pancreatitis (SAP) individuals. F) Receiver operating characteristic (ROC) curve analysis for the predictive power of ETA for distinguishing SAP (n = 10) from MAP (n = 15) group. Data are presented as mean ± SD. ns: not significant, p > 0.05; *: p < 0.05; **: p < 0.01; and ***: p < 0.001.

amine metabolites were up-regulated in the AP group (Figure 3B). The 19 differential metabolites between HC and AP groups with a fold change (FC) > 1.4, p < 0.05, and variable importance in the projection (VIP) values >1 are listed in Table S6. The top six metabolites with significant alterations (FC > 2) are topaquinone, spermidine, aminobutyraldehyde, adenine, arginine, and aminopropionaldehyde (Figure 3C). The two polyamine metabolites, spermine and spermidine, exhibited 1.5-fold and 2.7-fold up-regulation, respectively, in the AP group, which were consistent with polyamine catabolism being aggravated in the pancreas during SAP.[22] The changes in basic amino acids are also consistent with our recent investigation.[21] In particular, obvious alterations in two aromatic amines, topaquinone and dopaquinone, one dipeptide, Asp-Gly, and two amines, aminobutyraldehyde and aminopropionaldehyde, were detected for the first time in pancreatic samples. Additionally, we detected ETA in plasma, a

https://doi.org/10.1021/acs.analchem.4c06388
Anal. Chem. 2025, 97, 6611−6619

metabolite that is typically hard to analyze due to its lower levels in peripheral blood. It is notable that ETA changed between mild acute pancreatitis (MAP) and SAP in addition to the AP and HC groups (Figure S14). The levels of ETA in MAP and SAP were further determined as 0.061 ± 0.01 and 0.097 ± 0.006 μM (Figures 3D,E). The receiver operating characteristic curve of ETA exhibits AUC values exceeding 0.85 (AUC = 0.8533), which is essential for distinguishing SAP from MAP (Figure 3F). ETA occurs in every cell in the human body as the head of a group of PE and LPE, is highly distributed in the mammalian gastrointestinal tract, and its utilization dramatically affects lipid metabolism and short-chain fatty acid biosynthesis.[23] While the pancreas showed an overall decrease in glycerophospholipids, including PEs and LPEs, in a necrotizing AP mode.[24] Thus, ETA is essential for the molecular mechanism study, diagnosis, and management of SAP. The above findings indicate that amine metabolites alter dramatically in SAP, suggesting their potential value for diagnosing this disease.

On-Tissue Derivatization for MSI of Amine Metabolites. We also investigated the availability of NPU as an OTCD reagent for the MSI of amine metabolites in biological tissues. The strategy of on-tissue photochemical derivatization for MSI of amine metabolites in biological tissues is shown in Figure 4A. We further optimized the photocatalytic time, light wavelengths, concentration of derivatization reagents, and choice of solvent (Figure S15). Finally, we determined the optimal in situ reaction conditions at about 25 °C for 0.5 h with a 5 mg/mL NPU reagent, which shows good stability and precision (Figure S16). More significantly, we discovered that the light activation greatly influenced derivatization efficiency. Without on-tissue light activation, all amine metabolites cannot be detected by AFADESI-MSI (Figure 4B). After d_0-NPU photochemical derivatization, the sensitivity of amine metabolites in brain tissues is significantly improved (Figure S17). Due to the reaction efficiency of the photocatalytic reaction, no additional incubation is required to achieve good reaction efficiency, which provides the possibility of further reducing spatial displacement. Meanwhile, we tested the linearity of the analytical method. The linearity of the selected metabolites was around R^2 = 0.95 (Figure S18), and the structures of the metabolites were further identified by comparing the HRMS^2 spectrum of representative standards in MSI analysis (Figure S19). This isotope-labeled *in situ* absolute quantitative method also expands the possibility of an in-depth clinical application of the analytical method. Finally, we found 288 labeled derivatization peaks in brain and kidney tissues, of which 43 metabolites from brain tissue and 45 metabolites from kidney tissue were annotated by database or standard samples. MS images of some representative metabolites with significant *in situ* distribution in the brain and kidney are displayed in Figure 4C. Therefore, this derivatization strategy enables rapid and environmentally friendly analysis of amine metabolites via light activation, both for LC-MS and MSI platforms. The detailed advantages of this method over conventional derivatization techniques are further summarized in Table S7.

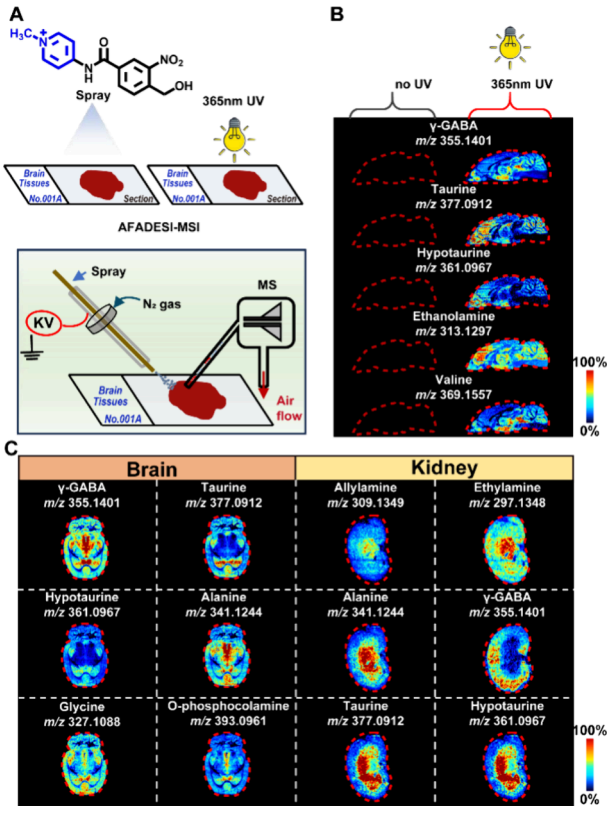

Figure 4. A) Schematic diagram of the on-tissue photochemical derivatization for MSI. B) MSI of representative amine metabolites in a sagittal brain section from wild-type mice with and without light activation. C) Representative MSI of d_0-NPU-derived amine metabolites in the rat brain and kidney.

Joint Analysis of Amine Submetabolome in Plasma and Tissue of Pancreatic Cancer. With the application of established methodologies, we determined the amine submetabolome in PC patients, who had both plasma and pancreatic tissue samples. Table S8 presents the demographic characteristics of PC patients included in this study. The spatial distribution of amine metabolites was visualized in PC (n = 8) and its distal paracarcinoma tissues (NT) group (n = 7) by OTCD. Figure 5A shows the H&E staining of PC and NT group, clearly revealing the pathological features of each. PC tissues exhibited a wide distribution of amine metabolites with significant changes under the OTCD conditions (Figure 5B). The PCA analysis of 207 paired MS peaks indicated different distributions of amine metabolites in PC and NT groups (Figure 5C), and almost 80% of the metabolites were up-regulated in the PC group (Figure 5D). Among them, 26 metabolites displayed a significant statistical difference between PC and NT groups with an FC > 1.4, p < 0.05, and variable importance in the projection (VIP) values >1 (Table S9 and Figure 5E). This suggests a reconfiguration of metabolism in PC cells that enhances biosynthesis.[25] Pancreatic stellate cells, which are associated with the tumor stroma, play a crucial role in the metabolism of PC by secreting nonessential amino acids, such as branched-chain amino acids, alanine, and Gly.[26,27] Our findings indicated elevated levels of Gly, alanine, and branched-chain amino acids within the tumor regions. Additionally, we observed increases in the level of aromatic amino acids such as phenylalanine, tryptophan, and tyrosine in the PC group. Notably, we detected significant elevations in less commonly reported metabolites, including methylamine, *o*-phosphocolamine, and LPE (20:4) specifically within the PC tissues. These results highlight the spatial distribution and tissue-specific alteration of amino acids and aliphatic amines in the PC and NT groups, providing insights into the reprogramming of amine metabolites and contributing

https://doi.org/10.1021/acs.analchem.4c06388
Anal. Chem. 2025, 97, 6611−6619

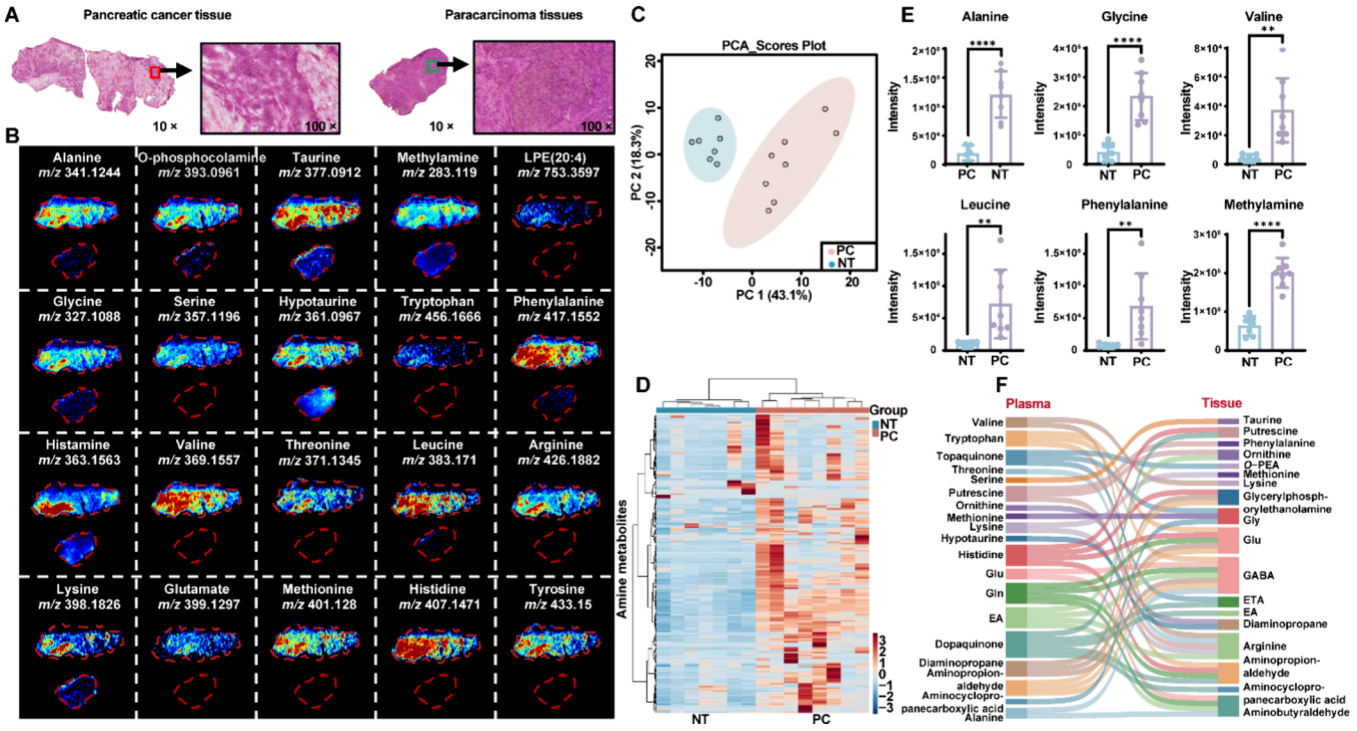

Figure 5. A) Hematoxylin-eosin (H&E) stain of pancreatic cancer tissue (PC, left) and paracarcinoma tissue (NT, right) sections. B) AFADESI-MSI visualization of common amine metabolites extracted from PC and NT after d_0-NPU derivatization. C) 2D score plot for PC and NT groups by PCA. D) Heatmap of mean normalized amine metabolite intensities in the pancreas of the PC group (n = 8) and NT group (n = 7). E) Representative expression levels of amine metabolites in PC and NT. F) Sankey diagram for the correlation of amines in plasma and tissue of PC patients.

to a deeper understanding of the molecular mechanisms underlying PC. Furthermore, we explored correlation of amine metabolites in plasma and tissue. We analyzed the amine submetabolome in the plasma of PC patients and HCs. The OPLS-DA results showed that there were significant differences between the two groups, and heatmap indicated the expression of more than 50% of amine metabolites was higher in PC than in HCs. The details of the metabolites are listed in Figure S20 and Table S10. Meanwhile, the peak intensities of primary amine derivatives for tissue and plasma were analyzed by Spearman analysis to identify the correlation of amine metabolites (Figure 5F). The results demonstrated significant correlations between metabolites involved in PE lipid metabolism such as glycerylphosphorylethanolamine (GPEA), ETA, and *o*-phosphocolamine. PE plays a crucial role in supporting the autophagic process, including the elongation of autophagosomes, and has been implicated in immune cell survival, apoptosis, and differentiation within tumors.[28,29] Interestingly, we found a negative correlation between tissue levels of methylamine and its concentration in plasma. Methylamine is produced endogenously from amine catabolism, with its tissue levels rising under certain pathological conditions. Its concentration is regulated by semicarbazide-sensitive amine oxidase, an enzyme significantly influencing glucose uptake and adipocyte differentiation, highlighting its physiological and pathological relevance.[30] In this context, alterations in methylamine concentrations deserve attention, as they may represent a promising differential metabolite in PC. Overall, these correlations could reflect a broader metabolic shift in amine metabolites during PC progression, suggesting their potential utility as biomarkers for early disease diagnosis. Further targeted biological investigations are warranted to elucidate the mechanisms driving amine alterations in PC patients alongside the development of appropriate animal models for future studies.

CONCLUSIONS

In summary, a novel photochemical derivatization strategy for amine submetabolome determination was developed on LC-MS and AFADESI-MSI platforms. Through rapidly forming an indazolone ring with various primary amines under UV light irradiation, the reagent displayed high reactivity, efficiency, and selectivity. Owing to the introduction of the 4-amino-1-methylpyridinium, the isotope tag, and two scan MS modes, the ionization efficiency, scope, and quantitation of amines have been significantly enhanced and enabled 423 peaks and 82 metabolites detected in biological samples by LC-MS. After semiquantitative analysis of the 82 amines in plasma from AP and HCs, resulting in the discovery of unreported aromatic amines, aminoaldehydes, and dipeptides with significant changes, followed by quantitative analysis of ETA allows for distinguishing the severities of AP. Notably, a significant improvement in the imaging sensitivity of amine metabolites was also achieved. Utilizing the established method, 43 metabolites from brain tissue and 45 metabolites from kidney tissue were visualized. It has good linearity and can be used for accurate quantification in MSI. Lastly, the strategy proposed above was successfully used to characterize both the amine metabolite profiling in plasma and spatially resolved alterations in the pancreatic tissues of PC patients. The discovery of metabolites characterizing *in situ* molecular lesions, such as methylamine, enhances the potential for amine-driven biomarker discovery in disease diagnosis. We are convinced that photochemical derivatization techniques will be powerful

https://doi.org/10.1021/acs.analchem.4c06388
Anal. Chem. 2025, 97, 6611−6619

in various submetabolomic fields in the future, particularly in the MSI platform. Further exploration of the related method is on the way in our laboratory.

■ ASSOCIATED CONTENT

Supporting Information

The Supporting Information is available free of charge at https://pubs.acs.org/doi/10.1021/acs.analchem.4c06388.

Additional experimental details, including ^{1}H and ^{13}C NMR spectra for the synthesis of d_0/d_3-NPU; Figures and Tables for the method setup of d_0/d_3-NPU coupled with LC-MS, Figures and Tables for the method setup of d_0/d_3-NPU coupled with MSI, and applications in clinical samples (PDF)

■ AUTHOR INFORMATION

Corresponding Authors

Dan Du − *Advanced Mass Spectrometry Center, Research Core Facility, Frontiers Science Center for Disease-related Molecular Network, West China Hospital, Sichuan University, Chengdu 610041, China*; orcid.org/0000-0001-9745-8197; Email: dudan1520@163.com

Chenggong Hu − *Department of Critical Care Medicine, West China Hospital, Sichuan University, Chengdu 610041, China*; orcid.org/0000-0002-1544-9930; Email: huchenggong@scu.edu.cn

Huimin Lu − *West China Centre of Excellence for Pancreatitis, Institute of Integrated Traditional Chinese and Western Medicine, Sichuan Provincial Pancreatitis Centre and West China-Liverpool Biomedical Research Centre, West China Hospital and Department of General Surgery, West China Hospital, Sichuan University, Chengdu 610041, China*; Email: hm.lu@scu.edu.cn

Authors

Yaling Wu − *Advanced Mass Spectrometry Center, Research Core Facility, Frontiers Science Center for Disease-related Molecular Network, West China Hospital, Sichuan University, Chengdu 610041, China*

Manjiangcuo Wang − *Advanced Mass Spectrometry Center, Research Core Facility, Frontiers Science Center for Disease-related Molecular Network, West China Hospital, Sichuan University, Chengdu 610041, China*

Rui Wang − *Advanced Mass Spectrometry Center, Research Core Facility, Frontiers Science Center for Disease-related Molecular Network, West China Hospital, Sichuan University, Chengdu 610041, China*

Shan Yang − *Department of Critical Care Medicine, West China Hospital, Sichuan University, Chengdu 610041, China*

Wanmeng Li − *Advanced Mass Spectrometry Center, Research Core Facility, Frontiers Science Center for Disease-related Molecular Network, West China Hospital, Sichuan University, Chengdu 610041, China*

Siwei Bi − *Department of Plastic and Burn Surgery, West China Hospital, Sichuan University, Chengdu, Sichuan 610041, China*

Xia Li − *Department of Critical Care Medicine, West China Hospital, Sichuan University, Chengdu 610041, China*

Yangjuan Bai − *Department of Laboratory Medicine, Research Centre of Clinical Laboratory Medicine, West China Hospital, Sichuan University, Chengdu 610041, China*

Qing Xia − *West China Centre of Excellence for Pancreatitis, Institute of Integrated Traditional Chinese and Western Medicine, Sichuan Provincial Pancreatitis Centre and West China-Liverpool Biomedical Research Centre, West China Hospital, Sichuan University, Chengdu 610041, China*

Complete contact information is available at: https://pubs.acs.org/10.1021/acs.analchem.4c06388

Author Contributions

[¶]Y.L.W. and M.J.C.W. contributed equally. D.D., Y.L.W., and M.J.C.W. designed the research; Y.L.W., M.J.C.W., W.M.L., S.W.B., R.W., S.Y., Y.J.B., and X.L. carried out the experiment; Y.L.W., M.J.C.W, W.M.L., and S.W.B. performed the data analysis; D.D., C.G.H., H.M.L., and Q.X. supervised the study; Y.L.W. and M.J.C.W. wrote the draft; D.D., C.G.H., and H.M.L. reviewed the manuscript. All authors have given approval to final version of the manuscript.

Notes

The authors declare no competing financial interest.

■ ACKNOWLEDGMENTS

We acknowledged the funding from National Natural Science Foundation of China (No. 82374256 to D.D.) and the Program of Science and Technology Department of Sichuan Province (No. 24SYSX0140 to H.L. and No. 2025ZNSFSC0992 to M.W.). These authors thank Pingxian Liu from the Laboratory of Human Diseases and Immunotherapy of West China Hospital, Sichuan University; Fei Fu, Na Jiang, Xiyu Wu and Qianlun Pu from the Mass Spectrometry Center of Frontiers Science Center for Disease-related Molecular Network of West China Hospital, Sichuan University; and Sisi Wu, Liqiang Hu and Zeliang Wei from Research Core Facility of West China Hospital, Sichuan University. All figures in this paper were exported with Adobe Illustrator and Microsoft PowerPoint as vector graphics. TOC graphic was created in BioRender. Han, D. (2025) https://BioRender.com/p58k420 (agreement number: CC27Z96V58).

■ REFERENCES

(1) Ling, Z. N.; Jiang, Y. F.; Ru, J. N.; Lu, J. H.; Ding, B.; Wu, J. *Signal Transduct Target Ther* **2023**, *8* (1), 345.

(2) Schepers, N. J.; Bakker, O. J.; Besselink, M. G.; Ahmed Ali, U.; Bollen, T. L.; Gooszen, H. G.; van Santvoort, H. C.; Bruno, M. J. *Gut* **2019**, *68* (6), 1044−1051.

(3) Trikudanathan, G.; Wolbrink, D. R. J.; van Santvoort, H. C.; Mallery, S.; Freeman, M.; Besselink, M. G. *Gastroenterology* **2019**, *156* (7), 1994−2007.e1993.

(4) Rahib, L.; Wehner, M. R.; Matrisian, L. M.; Nead, K. T. *JAMA Netw Open* **2021**, *4* (4), e214708.

(5) Siegel, R. L.; Giaquinto, A. N.; Jemal, A. *CA Cancer J. Clin* **2024**, *74* (1), 12−49.

(6) Luo, G.; Jin, K.; Deng, S.; Cheng, H.; Fan, Z.; Gong, Y.; Qian, Y.; Huang, Q.; Ni, Q.; Liu, C.; Yu, X. *Biochim Biophys Acta Rev. Cancer* **2021**, *1875* (2), 188409.

(7) Sandstrom, P.; Trulsson, L.; Gasslander, T.; Sundqvist, T.; von Dobeln, U.; Svanvik, J. *Amino Acids* **2008**, *35* (1), 225−231.

(8) Lee, M. S.; Dennis, C.; Naqvi, I.; Dailey, L.; Lorzadeh, A.; Ye, G.; Zaytouni, T.; Adler, A.; Hitchcock, D. S.; Lin, L.; Hoffman, M. T.; Bhuiyan, A. M.; Barth, J. L.; Machacek, M. E.; Mino-Kenudson, M.; Dougan, S. K.; Jadhav, U.; Clish, C. B.; Kalaany, N. Y. *Nature* **2023**, *616* (7956), 339−347.

(9) Ohara, Y.; Tang, W.; Liu, H.; Yang, S.; Dorsey, T. H.; Cawley, H.; Moreno, P.; Chari, R.; Guest, M. R.; Azizian, A.; Gaedcke, J.;

Ghadimi, M.; Hanna, N.; Ambs, S.; Hussain, S. P. *Cell Rep* **2023**, *42* (12), 113434.
(10) Garg, N.; Conway, L. P.; Ballet, C.; Correia, M. S. P.; Olsson, F. K. S.; Vujasinovic, M.; Löhr, J. M.; Globisch, D. *Angew. Chem., Int. Ed. Engl.* **2018**, *57* (42), 13805−13809.
(11) Zhang, T. Y.; Li, S.; Zhu, Q. F.; Wang, Q.; Hussain, D.; Feng, Y. Q. *Trac-Trends in Analytical Chemistry* **2019**, *119*, 115608.
(12) Plotka-Wasylka, J. M.; Morrison, C.; Biziuk, M.; Namiesnik, J. *Chem. Rev.* **2015**, *115* (11), 4693−4718.
(13) Guo, K.; Li, L. *Analytical chemistry* **2009**, *81* (10), 3919−3932.
(14) Liu, L.; Bao, G. Y.; Zhang, S. S.; Qin, Y.; Chen, X. P.; Wang, M. D.; Zhu, J. P.; Yin, H.; Lin, G. Q.; Feng, C. G.; Zhang, F.; Guo, Y. L. *Analytical chemistry* **2022**, *94* (50), 17606−17615.
(15) Guo, A. D.; Wei, D.; Nie, H. J.; Hu, H.; Peng, C.; Li, S. T.; Yan, K. N.; Zhou, B. S.; Feng, L.; Fang, C.; Tan, M.; Huang, R.; Chen, X. H. *Nat. Commun.* **2020**, *11* (1), 5472.
(16) Buchberger, A. R.; DeLaney, K.; Johnson, J.; Li, L. *Anal. Chem.* **2018**, *90* (1), 240−265.
(17) Harkin, C.; Smith, K. W.; Cruickshank, F. L.; Logan Mackay, C.; Flinders, B.; Heeren, R. M. A.; Moore, T.; Brockbank, S.; Cobice, D. F. *Mass Spectrom Rev.* **2022**, *41* (5), 662−694.
(18) Djambazova, K. V.; van Ardenne, J. M.; Spraggins, J. M. *Trends Analyt Chem.* **2023**, *169*, 117344.
(19) Soudah, T.; Zoabi, A.; Margulis, K. *Mass Spectrom Rev.* **2023**, *42* (2), 751−778.
(20) Zhu, J. S.; Kraemer, N.; Li, C. J.; Haddadin, M. J.; Kurth, M. J. *J. Org. Chem.* **2018**, *83* (24), 15493−15498.
(21) Pu, Q.; Wang, M.; Jiang, N.; Luo, Y.; Li, X.; Hu, C.; Du, D. *Anal. Chem.* **2023**, *95* (21), 8197−8205.
(22) Jin, H. T.; Lamsa, T.; Merentie, M.; Hyvonen, M. T.; Sand, J.; Raty, S.; Herzig, K. H.; Alhonen, L.; Nordback, I. *Pancreatology* **2008**, *8* (1), 15−24.
(23) Zhou, J.; Xiong, X.; Wang, K.; Zou, L.; Lv, D.; Yin, Y. *Curr. Mol. Med.* **2017**, *17* (2), 92−99.
(24) Yang, J.; Wang, M.; Qiu, Q.; Huang, Y.; Wang, Y.; Pu, Q.; Jiang, N.; Wang, R.; Wen, L.; Zhang, X.; Han, C.; Du, D. *Metabolites* **2023**, *13* (9), 993.
(25) Sousa, C. M.; Kimmelman, A. C. *Carcinogenesis* **2014**, *35* (7), 1441−1450.
(26) Sousa, C. M.; Biancur, D. E.; Wang, X.; Halbrook, C. J.; Sherman, M. H.; Zhang, L.; Kremer, D.; Hwang, R. F.; Witkiewicz, A. K.; Ying, H.; Asara, J. M.; Evans, R. M.; Cantley, L. C.; Lyssiotis, C. A.; Kimmelman, A. C. *Nature* **2016**, *536* (7617), 479−483.
(27) Zhu, Z.; Achreja, A.; Meurs, N.; Animasahun, O.; Owen, S.; Mittal, A.; Parikh, P.; Lo, T. W.; Franco-Barraza, J.; Shi, J.; Gunchick, V.; Sherman, M. H.; Cukierman, E.; Pickering, A. M.; Maitra, A.; Sahai, V.; Morgan, M. A.; Nagrath, S.; Lawrence, T. S.; Nagrath, D. *Nat. Metab* **2020**, *2* (8), 775−792.
(28) Hsu, P.; Shi, Y. *Biochim Biophys Acta Mol. Cell Biol. Lipids* **2017**, *1862* (1), 114−129.
(29) Debnath, J.; Gammoh, N.; Ryan, K. M. *Nat. Rev. Mol. Cell Biol.* **2023**, *24* (8), 560−575.
(30) Yu, P. H.; Wright, S.; Fan, E. H.; Lun, Z. R.; Gubisne-Harberle, D. *Biochim. Biophys. Acta* **2003**, *1647* (1−2), 193−199.

https://doi.org/10.1021/acs.analchem.4c06388
Anal. Chem. 2025, 97, 6611−6619